Analytical Viscous Flow Model and Test Validation of a Swirl Injector for Rocket Engine Application

Giuseppe Fiore^{1*}, Christian Bach^{2†}, Jan Sieder^{3†} and Martin Tajmar^{4†}
*Università di Pisa

†Technische Universität Dresden

¹g.fioredb@gmail.com; Via Caruso 8, 56122 Pisa, Italy

²christian.bach1@tu-dresden.de; Marschnerstrasse 32, 01307 Dresden, Germany ³jan.sieder1@tu-dresden.de; Marschnerstrasse 32, 01307 Dresden, Germany

Abstract

The generally adopted flow model inside a swirl injector, widely used injection concept for propulsive applications, relies upon the hypothesis of ideal flow neglecting the fluid viscosity effects. This model showed significant prediction errors with relatively high viscosity propellants, often leading to the need of an experimental characterization of the injection elements. In this paper an analytical approach is presented, which includes the effects of viscous diffusion on the injector performance leading to a close form flow solution. The built model is thus experimentally validated testing a LOX and an Ethanol injector: the good agreement between the model and the experimental results leads to the construction of the injectors operational maps describing the injector behaviour even in the presence of viscous effects.

Nomenclature

A_{film} A_N β C Δp δ^* dS φ h_{sw} L l_{sw} m	 Fluid film cross sectional area Injector nozzle cross sectional area Flow spread angle Dimensionless circulation Injector pressure drop Displacement thickness Surface element Passage fullness coefficient Swirling film thickness Characteristic flow length Swirl chamber wetted path length Mass flowrate Viscous flowrate defect 	\Re Re Re_{sw} Re_x r_{gc} r_{in} R_{in} R_{sw} ρ ϑ U	= = = = = = = = = = = = = = = = = = = =	Trajectory radius of curvature Reynolds No. Swirl chamber Reynolds No. Streamwise coordinate Reynolds No. Gaseous core radius Tangential inlets radius Chamber swirl arm Injector nozzle radius Swirl chamber radius Fluid density Azimuthal coordinate Characteristic flow velocity Unperturbed velocity profile
			_	
•	•		=	3
L	•		=	
l_{sw}			=	Azimuthal coordinate
•	= Mass flowrate	U	=	Characteristic flow velocity
\dot{m}_{defect}	= Viscous flowrate defect	u_0	=	Unperturbed velocity profile
\dot{m}_{ideal}	= Ideal flowrate	$u_{(y)}$	=	Stratified velocity profile
μ	= Massflow coefficient	v	=	Azimuthal velocity
μ_l	= Fluid viscosity	V	=	Total velocity
μ_{vis}	= Viscous massflow coefficient	V_N	=	Total velocity in the injector nozzle
n	= Number of tangential inlets	x_{sw}	=	Swirl path coordinate
p_c	= Combustion chamber pressure	z_N	=	Injector axial length
p_{feed}	= Injector feeding pressure			

⁴ martin.tajmar@tu-dresden.de; Marschnerstrasse 32, 01307 Dresden, Germany

1. Introduction

The use of a swirl injector to feed the combustion chamber of a rocket engine has proven to be a powerful choice in terms of atomization and mixing efficiencies [1], combustion stability margin and throttleability [2] together with high massflow per element. These features are gained through the tangential introduction of the propellant in the swirl chamber that realizes an angular momentum-driven flow development.

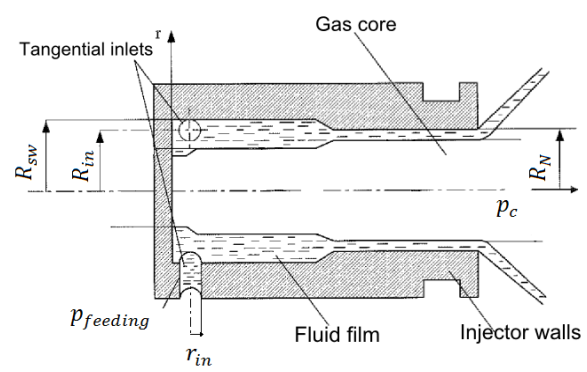


Figure 1: Swirl injector scheme [1] (modified)

Nevertheless the high fluid/wall interfacial areas make this injection concept very sensitive to viscosity effects [2] since the Boundary Layer (BL) height can become comparable to the dimensions of the spreading propellant film thickness.

The existing flow model, developed in the late 1970s by Bazarov [1], relies upon the hypothesis of inviscid flow: solving the flow equation in this frame gives in fact the possibility to correlate the applied pressure drop Δp to the expelled massflow \dot{m} by means of a dimensionless coefficient μ known as massflow discharge coefficient.

$$\dot{m} = \mu \, \pi R_N^2 \sqrt{2\rho \Delta p} \tag{1}$$

where R_N is the radius of the injector outlet as shown in Figure 1 and ρ is the density of the driven propellant. Defining two other dimensionless groups, the dimensionless circulation C and the film passage fullness coefficient φ as:

$$C = \frac{R_N R_{in}}{n \, r_{in}^2} \tag{2}$$

and

$$\varphi = \frac{A_{film}}{A_N} = 1 - \left(\frac{r_{gc}}{R_N}\right)^2 \tag{3}$$

the Bazarov inviscid theory is able to correlate the massflow coefficient μ to the injector geometrical features:

$$\mu = f(R_N, R_{in}, r_{in}, n) \tag{4}$$

where R_N , R_{in} , r_{in} are the radii of the nozzle outlet, the injection arm and the tangential inlets respectively, geometrical dimensions of the injector as shown in Figure 1. n is the number of tangential inlets, A_{film} and A_N are the cross sectional areas of the fluid film and the nozzle outlet and r_{gc} is the gaseous core radius. Experimental data for this injection concept has been obtained within the SMART Rockets project [4], in which a 500 N liquid propellant engine is designed with the goal of propel a payload-carrying sounding rocket [8]. This engine in fact features a coaxial swirl injector assembly in which Liquid Oxygen (LOX) and Ethanol are driven to feed an oxide ceramic matrix composite (OCMC) combustion chamber. Experimental data obtained with LOX and Ethanol, two fluids with relatively low and high viscosities (see Table 1), confirm the good prediction accuracy of the Bazarov

model in the low viscosity case while significant deviations are observed in the second case [3] (see Section 4). This prompts viscous diffusion effects to be the cause of the mismatch between the ideal theory and the experiments and at the same time highlights the need for a model accounting for the fluid viscosity to characterize the injector with a pressure-massflow correlation.

Table 1: Propellants viscosities [5,6]

	LOX_{sat}	$LN2_{sat}$	Ethanol
$\mu_l(@10\ bar)[mPa\ s]$	0.097	0.075	1.17
$\mu_l(@20\ bar)[mPa\ s]$	0.082	0.05	1.25

In this paper an analytical approach to account for viscosity effects on the injector discharge capability is presented: the BL structure inside the swirl chamber is modelled in terms of the ideal flow parameters obtaining a close form solution for the viscous discharge coefficient. The obtained results avail to build the operative map of the swirl injector that is then compared to experimental data obtained via cold flow testing of the injectors.

2. Viscous flow model

The first step for the inclusion of viscous effects into the flow model is to give a proper definition of the Reynolds number for the flow. This dimensionless parameter in fact displays the relative importance of inertial and viscous effects acting in the problem:

$$Re = \frac{Inertial\ Force}{Viscous\ Force} = \frac{\rho UL}{\mu_{I}} \tag{5}$$

Being U and L the characteristic velocity and length of the flow and μ_l the viscosity of the fluid. In order for this parameter to be representative of the flow viscous behaviour, appropriate values should be chosen for the characteristic length and velocity. With reference to Figure 2, by definition of Reynolds number what matters is the length across which the fluid is pushed by the inertial forces. In this particular flow configuration this length is well represented by the film thickness h_{sw} while, due to the 3D nature of the problem, the reference velocity should be taken as the total velocity V.

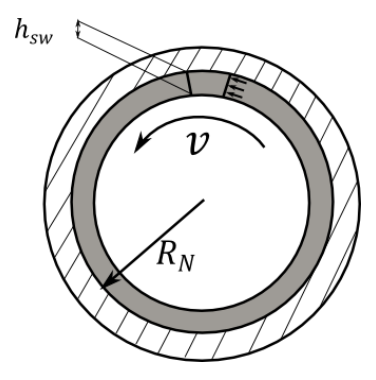


Figure 2: Flow configuration

Specializing the thickness and the velocity inside the injector nozzle so to earn ease of representation still keeping the same meaning, and rearranging the Reynolds definition with the help of the ideal flow relations [1] and Equation (1), the overall Reynolds number inside the swirl chamber can be defined as function of the injector mass flowrate:

$$Re_{sw} = \frac{\rho V_N h_{sw}}{\mu_I} = \frac{\varphi \dot{m}}{2\pi \mu R_N \mu_I} \tag{6}$$

Where the thickness of the annular section has been expressed using the thin annulus approximation valid for $h_{sw} \ll R_N$ (if this hypothesis does not hold the actual thickness is computed without simplifications) and the definition of passage fullness coefficient φ :

$$A_{film} = \varphi \pi R_N^2 = \pi R_N^2 - \pi (R_N - h_{sw})^2 \approx 2\pi R_N h_{sw}$$
 (7)

Hence:

$$h_{sw} = \frac{\varphi R_N}{2} \tag{8}$$

As an example, Table 2 shows the value of the defined swirl Reynolds No. for different flows of Liquid Nitrogen (LN2), LOX and Ethanol, specified for the LOX and Ethanol injectors built within the SMART Rockets project [8].

Table 2: Swirl Reynolds

	LOX	LN2	Ethanol
Re_{sw} (@10 bar, 125 g/s)	197 200	255 000	12 600
$Re_{sw}(@20\ bar, 125g/s)$	232 000	382 600	12 000

The values of the Reynolds No. confirm what has been observed in the injectors tests: for LOX and LN2 the Reynolds No. is one order of magnitude higher than the one of the Ethanol, no sensible viscosity effects should be noticed so that the inviscid model should be capable of accurately predicting the empirical results. The opposite happens on the Ethanol line since the very low Reynolds, justified by higher viscosity of the fluid, makes the problem difficult to be realistically described when neglecting viscosity effects that play an important role in the flow development.

What happens is that viscous diffusion causes a massflow reduction through the injector because of the velocity stratification near the wall. The non-slip condition at the wall forces the particles entrained in the flow near the swirl chamber wall to have zero velocity, but moving away from the injector surface the flow gains its nominal velocity since viscosity effects are confined in the vicinity of the wall. This cause a stratification of the velocity profile that can no longer be considered uniform but radially varying. Recalling the concept of the Boundary Layer theory, it can be stated that being the BL a region near the solid wall where all the viscosity effects are confined, the velocity varies from zero at the wall to the inviscid value at the BL edge since outside the BL no viscosity effect is felt thus the fluid behaves as it would in an inviscid flow (Figure 3).

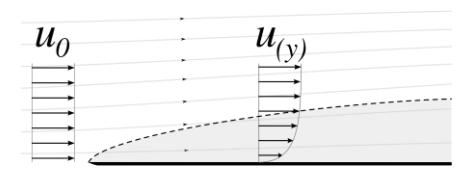


Figure 3: Boundary Layer theory

The consequence of the viscosity-induced velocity profile stratification is that, in the viscous case, the massflow entrained in the BL thickness is actually lower than the one that would be entrained in the same length in an inviscid flow. Since the velocity outside the BL is uniform and equal in both cases, it can be stated and verified by direct integration that the overall massflow in the viscous case is reduced because of viscous diffusion effects:

$$\int_{viscous}^{h} \rho \vec{V}(r) \cdot \vec{dS} < \int_{inviscid}^{h} \rho \vec{V} \cdot \vec{dS}$$
(9)

The curious fact is that this process of massflow reduction takes places in both Ethanol and LOX flows with the same mechanism: however being the BL height inversely proportional to the square root of the Reynolds No., in the LOX flow *Re* is so high that viscosity effects are confined in an extremely thin region near the wall, so that the decrease in massflow becomes negligibly small. This rather simple explanation of the viscous diffusion in the injector flow well describes what has been observed experimentally for the two different flows.

The focus is therefore shifted in finding the velocity distribution in the BL and use (9) to obtain the massflow defect. In particular what matters is the BL profile at the end of the injector duct: the BL thickness increases along the axial coordinate of the injector and the representative figure for the mass defect is the integration of the velocity profile at the injector outlet, where the viscosity-dominated region has the highest thickness. A convenient choice that suites this problem could be the use of the definition of the BL displacement thickness δ^* . This characteristic length value is the thickness that should be added to the wall (or equivalently deprived to the flow near the wall) in order to obtain an equivalent uniform flow, with uniform velocity equal to that outside the BL, whose massflow equals the one that would be obtained by integration of the actual velocity profile, as sketched in Figure 4.

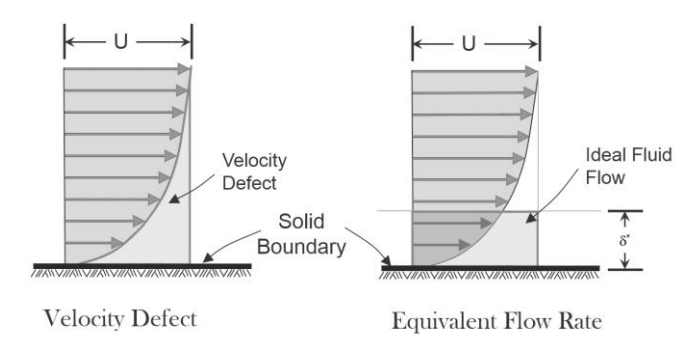


Figure 4: Boundary Layer displacement thickness [10]

The next step would be to evaluate the displacement thickness at the injector outlet and then treat the flow inside the injector as uniform like in the inviscid case, but on a fictitious geometry in which the wall is shifted by a δ^* length. In this way, the massflow flowing through this fictitious geometry is the actual massflow through the injector including viscous mass defects.

Evaluation of the boundary layer mattering thicknesses is however not a trivial challenge, especially due to the 3D nature of the flow configuration. Anyway known solutions for pretty different flow configurations can be taken as reference. The relevant differences in terms of geometric and fluid-dynamic effects between the actual and the reference flow configurations can thus be discussed to assess the limits of validity and the differences that those effects bring on the growth of the BL thickness, that is the primary quantity of interest. The Blasius solution for the BL developing across a flat plate flow can be taken as a reference: in this simple flow configuration no pressure gradients are experienced so that the BL grows naturally with the flow coordinate. The solution for the growth of the displacement thickness as function of the flow coordinate is [9]:

$$\delta^*(x) = 1.7208 \frac{x}{\sqrt{Re_x}} = 1.7208 \sqrt{\frac{\mu_l x}{\rho V}}$$
 (10)

where the x coordinate represents the portion of the wall length wetted by the fluid. The different factors influencing the growth of the BL in the actual configuration w.r.t. the reference one come from two effects:

- Presence of a negative axial pressure gradient toward the injector nozzle due to propellant acceleration
- Effect of curvature developing centrifugal forces inside the flow

The first effect is usually beneficial in terms of growth of the BL since negative pressure gradients along the streamwise direction are stabilizing and retard the BL's thickness growth. The second effect require a little bit more attention since centrifugal forces set up due to the convex curvature build up a radial pressure stratification, according to the local equilibrium of a flow element, the pressure differential in the radial direction is:

$$(dp)_r = \rho \frac{V^2}{\Re} dr \tag{11}$$

where \Re is the local radius of curvature of the flow, of the order of the chamber radius and depending on the axial-to-azimuthal velocity ratio. The important fact is that the pressure gradient in the radial direction is positive, meaning that the flow is pushed against the wall by centrifugal effects (centrifugal pumping), leading to a further decrease of the BL thicknesses w.r.t. the reference ones.

As a result, inclusion of the effects of the different flow configuration w.r.t. the Blasius one gives that the BL's properties, in particular the displacement thickness, grow in a slower fashion with the flow coordinate meaning that the use of the Blasius profile turns up in a conservative overestimation of the viscosity effects. This fact is really encouraging because if it were the opposite, namely the BL thickness was underestimated, the Blasius model could no longer have been used because the faster growth of the BL in the injector would have probably lead to separation of the flow, condition at which the BL behaves in a totally different fashion w.r.t. the reference one.

Drawing conclusions the use of a Blasius profile still well describes the mechanisms that lead to the massflow defect bringing an acceptable overestimation of the BL thicknesses with the advantage of a handy analytical solution amenable to be easily accommodated into the swirl injector flow model. Accordingly, the BL's displacement thickness for the swirl injector can be expressed in a convenient way using the definition for Re_{sw} (6) and the film thickness (8):

$$\delta^*(x_{sw}) = 1.7208 \sqrt{\frac{\mu_l x_{sw}}{\rho V_N} \frac{h_{sw}}{h_{sw}}} = 1.7208 \sqrt{\frac{\varphi R_N x_{sw}}{2Re_{sw}}}$$
(12)

Where the coordinate x_{sw} is now the curvilinear abscissa of the helical path of the flow through the swirl chamber, representing the length of the wet wall's surface. This is the mattering length for the evaluation of the BL growth along the path of the fluid inside the injector, as sketched in Figure 5.

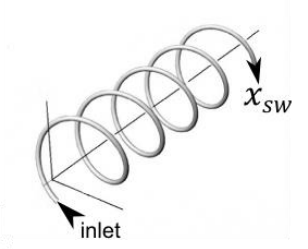


Figure 5: Helical path of the swirling flow inside the injector

This parameter can be found by geometrical considerations about the helical-like pattern of the flow, as it is intuitive the shorter the pitch of the helix, the longer the wet surface and vice versa, since the axial length of the helix is fixed by the injector size. An exact characterization of the swirled path can be done with the help of the inviscid theory using the result for the spread angle or equivalently the axial-to-total velocity ratio. The use of the inviscid theory for the evaluation of the path turns to be helpful in obtaining a "linearized" viscous result as a correction of the inviscid one that stands as a reference.

In a cylindrical reference frame the parametric equation of a helical curve of radius R, pitch p and azimuth ϑ is:

$$\begin{cases} x = R\cos\theta \\ y = R\sin\theta \\ z = \frac{p}{2\pi}\theta \end{cases} \tag{13}$$

The spread angle β of the helix can be related to the inviscid flow parameters via (14) and, by geometrical analysis, the relation holding between the pitch and the spread angle is (15):

$$\cos\beta = \frac{w}{V} = \frac{\mu}{\varphi} \tag{14}$$

$$tan\beta = \frac{2\pi R}{p} \tag{15}$$

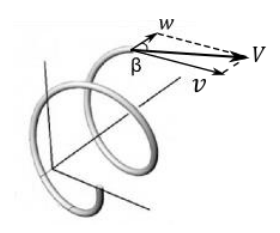


Figure 6: Velocity ratio and spread angle

The goal of the geometrical analysis is to find the variation of the flow coordinate x_{sw} and in particular its value at the end of the nozzle ($z = z_N$) as a function of the flow parameters. This length can be found by straight integration of the helix equation; with few calculus it is obtained:

$$l_{sw} = \int_0^{x_{sw}(z_N)} ds \tag{16}$$

With:

$$ds = \sqrt{dx^{2} + dy^{2} + dz^{2}} = dz \sqrt{\left(\frac{2\pi R}{p}\right)^{2} + 1} = dz \sqrt{\tan^{2}\beta + 1} = \frac{dz}{\cos\beta}$$
 (17)

And with the variable substitution the wet path length $l_{sw} = x_{sw}(z_n)$ is obtained:

$$l_{sw} = \int_0^{z_N} \frac{dz}{\cos\beta} = \frac{\varphi}{\mu} z_N \tag{18}$$

Hence, it is now possible to express the displacement thickness evaluated at the nozzle outlet section, leading parameter for the expression of the viscous mass defect:

$$\delta^*(z_N) = 1.7208 \sqrt{\frac{\varphi R_N l_{sw}}{2Re_{sw}}}$$
 (19)

Being able to pass into the equivalent uniform flow in which the wall thickness is shifted by a displacement thickness length, and remaining in the thin film approximation, the defect massflow can be found via a simple proportion. In fact, dealing with uniform flows, the defect massflow and the displacement thickness stand in the same relation of the ideal massflow and the total thickness film, the same can be stated for the massflow coefficients:

$$\frac{\dot{m}_{defect}}{\delta^*} = \frac{\dot{m}_{ideal}}{h_{sw}} \quad \Rightarrow \quad \dot{m}_{defect} = \frac{\delta^*}{h_{sw}} \dot{m}_{ideal} \tag{20}$$

Hence, with the definition (8) of the film thickness:

$$\dot{m}_{vis} = \dot{m}_{ideal} - \dot{m}_{defect} = \dot{m}_{ideal} \left(1 - \frac{2\delta^*}{\varphi R_N} \right) \tag{21}$$

Finally using (19) the relation for the viscosity-corrected massflow discharge coefficient writes:

$$\mu_{vis} = \mu \left(1 - 1.7208 \sqrt{\frac{2l_{sw}}{\varphi R_N Re_{sw}}} \right) \tag{22}$$

This relation finally gives the massflow coefficient of the injector accounting for viscous losses. The new dimensionless parameter μ_{vis} has the same task of the ideal one for performance prediction: relate the pressure drop

to the massflow established in the injector via (1). This time the massflow coefficient does not only depend on the injector's basic geometry like it was in the ideal model.

The longitudinal dimension of the injector is considered since it fixes the length of the wet surface on which viscous effects act. There is also a massflow dependence through the swirl Reynolds No.: the higher the velocity of the flowing fluid the slower the growth of the BL, meaning that going towards higher massflows (increasing Re) the viscosity effects are less and less important. Substitution of the Re_{sw} definition (6) into (22) allows to plot the μ_{vis}/\dot{m} characteristic curve and compare it to the inviscid theory.

Figure 7 shows the trend of the massflow coefficients of the LOX and Ethanol injectors compared to the ideal theory.

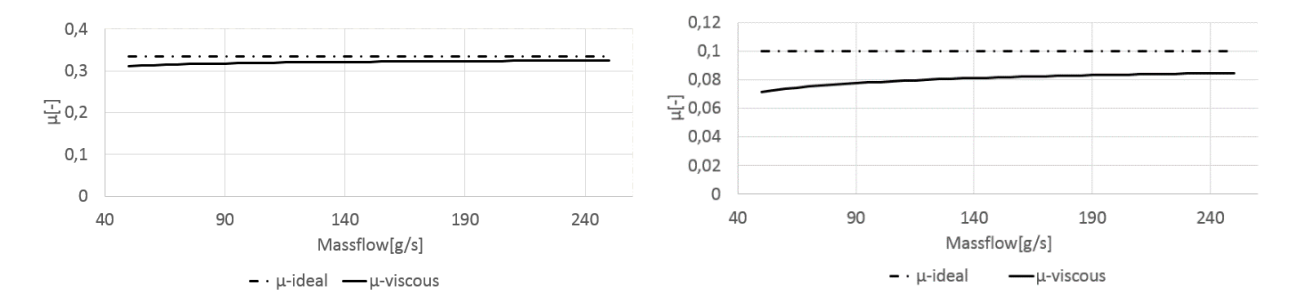


Figure 7: LOX (left) and Ethanol (right) ideal and viscous discharge coefficients

As Figure 7 shows there is no sensible shift between ideal and viscous model on the LOX injector, the low viscosity and in particular the high Reynolds No. realized in the injector makes the ideal model an accurate tool for the injector performance prediction. A different situation is depicted on the Ethanol injector, ideal and viscous models give conflicting results leading to an evident shift in the massflow coefficient prediction. Even the trend of increase the discharge capability toward high massflows is more pronounced emphasizing the Ethanol injector sensitivity to Reynolds No. changes.

3. Experimental set-up

To validate the built viscous model the experimental apparatus realized within the SMART Rockets project [7] has been set for the cold flow testing of the injectors. A scheme of the test bench is shown in figure 8.

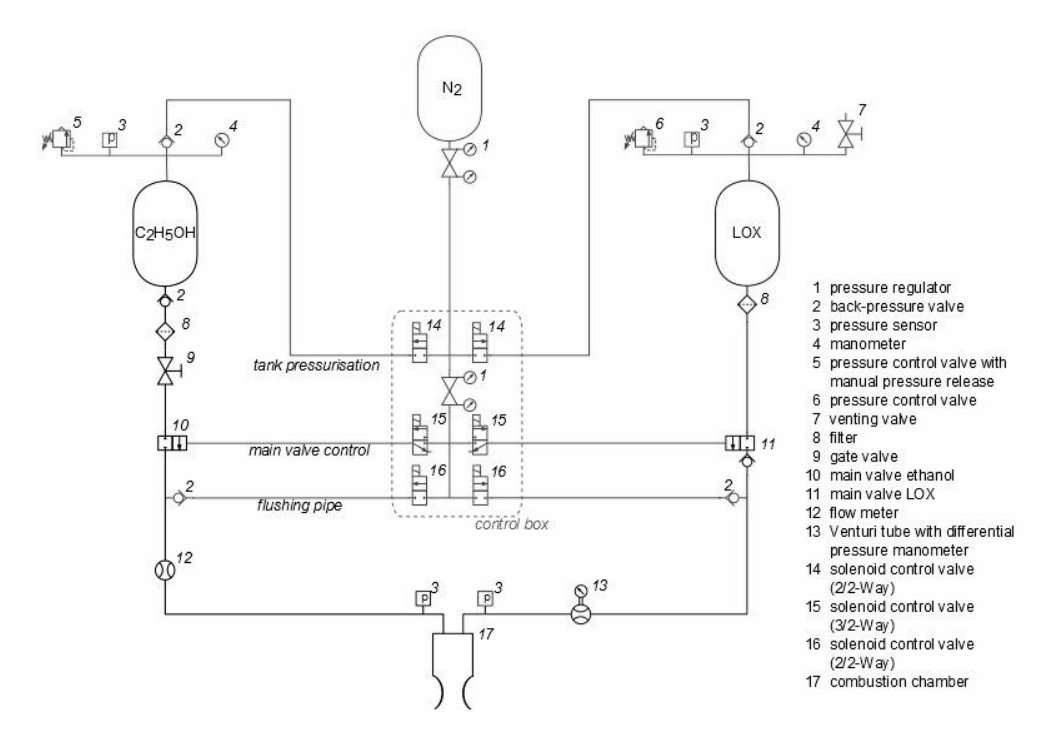


Figure 8: Test bench scheme [7]

The test facility built for the sake of testing a 500 N LOX-Ethanol propelled engine, features two propellant tanks for the LOX (cryogenic proven) and Ethanol respectively, both pressurized by a gaseous Nitrogen tank and connected with the injectors. Several sensors are installed on the propellants lines: temperature sensors are mounted in the LOX tank in order to control the vapor fraction and monitor the fueling cycles of the cryogenics, pressure sensors are mounted inside the tank and before the injectors in order to control the line pressures. Massflow sensors on each line measure the flowrates and in particular, the LOX massflow sensor is also able to measure the fluid density accounting for vapor presence in the cryogenic that always works near saturation conditions.

The connection between the test bench and the injector has been realized using a copper pipe on the Ethanol line and a thermally insulated pipe on the LOX line, insulation of the LOX line and cooling cycles proved in fact to be a critical challenge for obtaining vapor free shots of the cryogenic during the test campaigns. Figure 9 shows the CAD section views of the two injectors used for the tests.



Figure 9: CAD section view of the LOX (left) and Ethanol (right) injectors [3]

Both injectors are fed via 3 tangential inlets connected to the feeding lines of the test bench and are designed to work in a coaxial fashion.

The manufacturer of the pressure sensors claims a measurement error of 0.2 bar while the maximum massflow error is 5 g/s, satisfactory values since the tests are realized in the neighborhood of 10 bar pressure and 150 g/s massflow, way far from the sensor error range. Attention should be paid to realizing stable and steady flows since both results of ideal and viscous theory were obtained under the hypothesis of steady flow field.

4. Test results

The test campaign has been conducted using Ethanol and the simulant fluid LN2 in place of LOX for safety reasons. Being LN2 a cryogenic fluid with similar transport properties of LOX the results can be reliably scaled. The injectors have been tested in two different cold flow fashions, single flow and combined Ethanol-LN2 flow in order to check if any mutual throttling effect exists when the two injectors work in the coaxial fashion, providing a mixing zone to the fluids before the jet expulsion. Arranged the test bench for the particular test to be run, several shots were obtained with the goal of reaching steady-state conditions for a representative time interval. The cryogenic shots were always preceded by cooling pre-shots in order to cool down the LOX line obtaining shorter settling time for the fluid to become vapor-free, realizing thus steadier test runs.

For both the prescribed flow fashion a pressure range 5-to-20 bar has been covered with a corresponding massflow range 50-to-200 g/s in order to conveniently simulate the range of interest for the rocket engine the injectors belong to.

Steady state values of pressures, massflows and densities are evaluated and compared to the ideal and viscous predictions and Equation (1) is used with the measured data to obtain the observed values of the massflow coefficients. The first result obtained is that no sensible throttling effect has been observed with the injectors working in combined flow fashion. This is an important result since the combined flow fashion is the actual working

condition of the injectors in the engine. The absence of mutual throttling effects means that in the design phase the operative map of each injector can be used by itself in order to set the geometric and pressure parameters, then the injectors can be assembled maintaining the same pressure-flowrate relations.

Results in terms of massflow coefficient are shown in Figure 10 and 11 [3], for the LOX injector are also displayed previous results obtained with LOX cold flow tests.

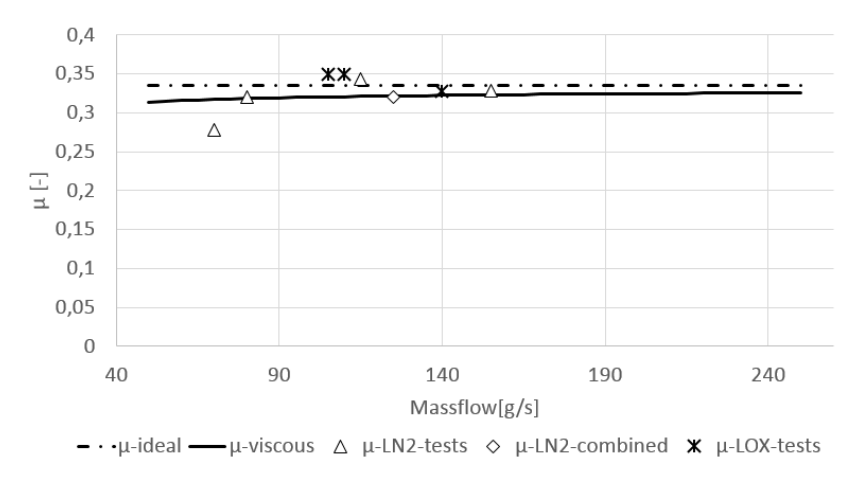


Figure 10: LOX injector test results

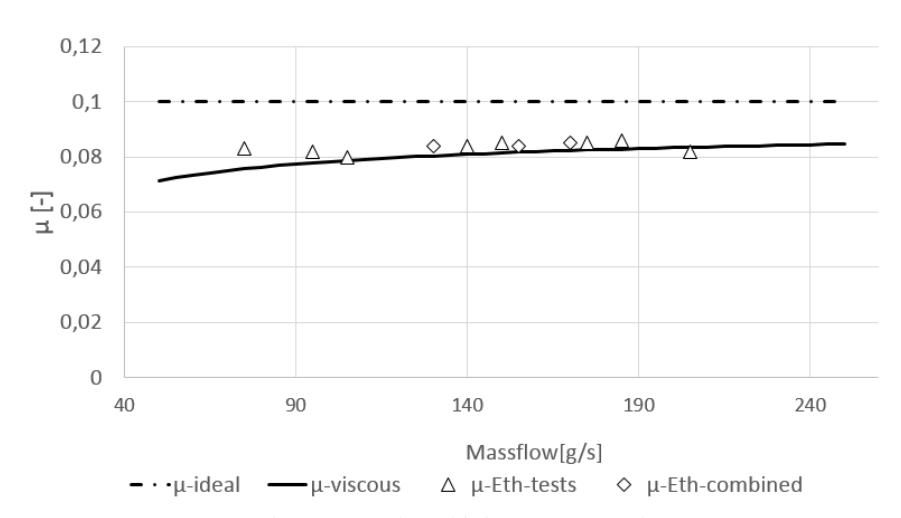


Figure 11: Ethanol injector test results

- The LOX injector results show a good agreement between empirical observation and theory, once again there is no substantial difference between ideal and viscous theory given the high values of the Reynolds No. for this kind of flow. A certain degree of scattering of the test results is observed, due to the density fluctuations of the cryogenics, symptom of a certain vapor fraction in the fluid also confirmed by the slightly lower density observed, especially in the lower massflow range, index of lower injection pressure thus reduced saturation temperature of the cryogenic.
- Results obtained with the Ethanol injector confirm with excellent accuracy the viscous theory: in addition to being very close to the predicted values, the test results confirm the trend of discharge capability reduction towards decreasing flowrates indexes of lower Reynolds numbers thus higher influence of viscous effects in the flow. In addition, the analytical prediction slightly underestimates the discharge coefficient (overestimates the viscous effects) and this is in accordance with the hypotheses holding behind the viscous model, in particular the use of a Blasius BL profile parametrized around the swirl path. This assumption in fact neglects the beneficial pressure gradients coming from the fluid centrifugation that retard the growth of the BL slightly increasing the discharge capability of the injector.

Using the new definition of the discharge coefficient (22) it has been possible to build the new pressure-massflow correlation and design the operational maps of the injectors. Figure 12 and 13 shows the operative maps of both injectors together with the obtained test results highlighting the difference between ideal map and viscous map [3].

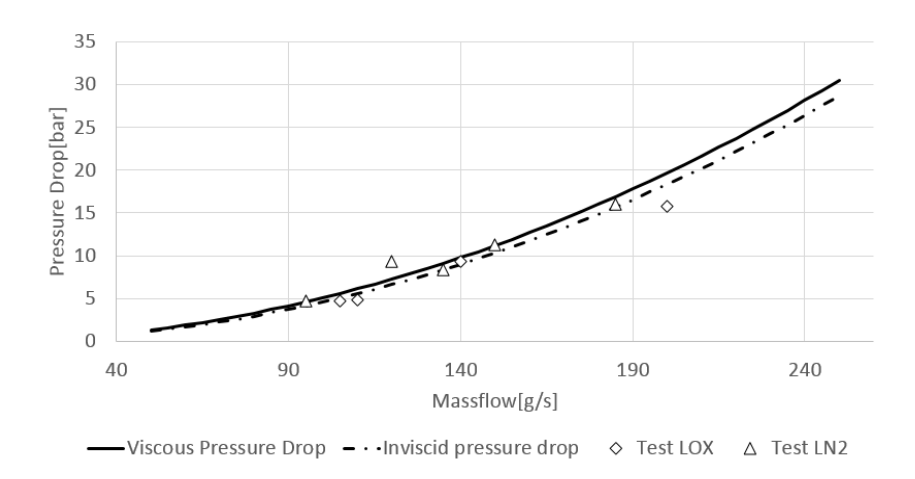


Figure 12: LOX injector map

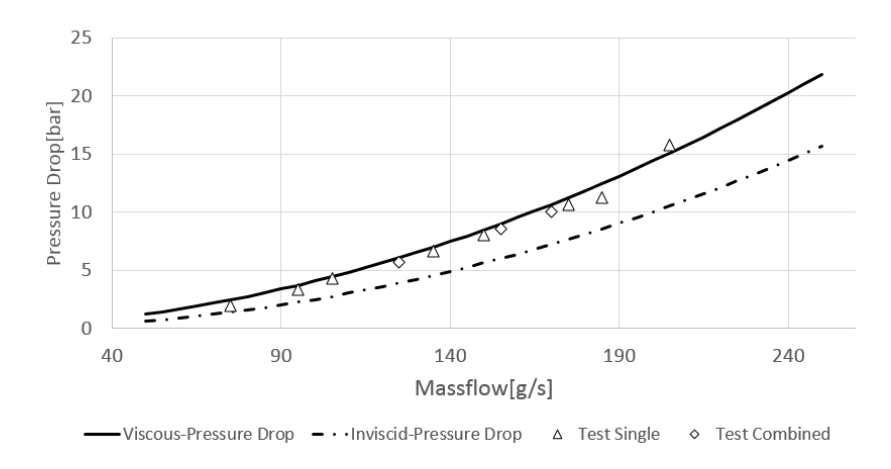


Figure 13: Ethanol injector map

5. Conclusions

A viscous flow model has been built for the swirl injector, obtaining an analytical expression for the massflow discharge coefficient, depending both on the injector geometrical features and on the fluid's transport properties that characterize the flow Boundary Layer structure. A cold flow test campaign on the injector has been conducted and confirmed the predictions of the viscous flow model: test results confirmed with excellent accuracy the viscous predictions also highlighting the influence of the Reynolds regime on the injector discharge capability. This is observed very clearly in the Ethanol injector since no substantial difference between ideal and viscous flow model holds for the low viscosity case of the LOX injector. Through the definition of the viscous discharge coefficient the injectors have been characterized via pressure-massflow correlations, key aspect for the design phase of the injector themselves and for the assignment of the line pressures in the propulsion assembly, otherwise done in an experimental way to account for the inappropriateness of the ideal model to describe highly viscous flows. The presented model represents thus a powerful tool for the understanding and design of this injector concept even when propellant viscosity effects cannot be neglected.

Acknowledgements

The authors would like to thank Dr. Olaf Przybilski, team leader of the project, and all the "SMART Rockets" student team of the "TU Dresden" for their support during the experimental phase; Ing. Maximilian Nürnmberger, responsible for the test bench control; Prof. Luca D'Agostino of "Università di Pisa" and Ing. Lorenzo Vallini for their wise suggestions during the paper writing phase.

References

- [1] Bazarov V., Yang V., Puri V. 2004. Design and dynamics of jet and swirl injectors. AIAA Progress in astronautics and aeronautics Vol. 200, 13-103.
- [2] Zong N., Yang V. 2008. Cryogenic fluid dynamics of pressure swirl injectors at supercritical conditions. Physics of Fluids 20.
- [3] Fiore G. 2015. Design of the flight version combustion chamber head and coaxial swirl injector for a LOX-Ethanol rocket engine. Università di Pisa/TU Dresden, STERN Project documentation.
- [4] Bach C., Sieder J., Przybilski O. 2014, STERN Project documentation. TU Dresden
- [5] Hanley M., McCarty R. D., Haynes W.M. 1974. The viscosity and thermal conductivity coefficients for dense gaseous and liquid Argon, Krypton, Xenon, Nitrogen and Oxygen. Cryogenic division, National Bureau of Standards.
- [6] Tanaka Y., Matsuda Y. 1987. Viscosity of water+alcohol mixtures under high pressure. International journal of thermophysics No.2.
- [7] Bach C., Sieder J., Przybliski O., Tajmar M. 2013. Smart Rockets: development of a 500 N LOX/Ethanol-sounding rocket for the DLR STERN programme. Deutscher Luft-und Raumfahrtkongress 2013.
- [8] Bach C., Sieder J., Nürnmberger M., Voigt N., Przybliski O., Tajmar M. 2014. Proceedings of the SMART Rockets project: design development and first measurement results of a 500 N LOX/Ethanol combustion chamber. Deutscher Luft-und Raumfahrtkongress 2014.
- [9] Blasius H. 1908. Grenzschichten in Flüssigkeiten mit kleiner Reibung. Z. Math. Phys. 56 1-37.
- [10] Goyal R. 2013. Boundary Layer equations. Malaviya National Institute of Technology.
- [11] Yang V., Habiballah M., Hulka J., Popp M. 2004. Liquid rockets thrust chamber: aspects of modelling and design. AIAA Progress in astronautics and aeronautics Vol. 200.
- [12] Eberhart C., Lineberry D., Moser M. 2010. Effects of variable chamber pressure on a swirl coaxial injector: a cold flow study. AIAA 2010-6665.